applied sciences

MDPI

Article

The Ultimate Strength of Fully Transparent Pressure-Resistant Spherical Cabins

Fang Wang [1,*], Youjie Li [1], Zhihao He [1], Bingxiong Zhao [2,3], Jinfei Zhang [1] and Yu Wu [1]

[1] College of Engineering Science and Technology, Shanghai Ocean University, Shanghai 201306, China; liyoujie19970508@icloud.com (Y.L.); zhihaohe1226@163.com (Z.H.)
[2] School of Marine Engineering, Jimei University, Xiamen 361021, China
[3] Naval Architecture and Shipping College, Guangdong Ocean University, Zhanjiang 524088, China
* Correspondence: wangfang@shou.edu.cn

Abstract: The fully transparent cabin used in a manned submersible is typically made of the viscoelastic material polymethyl methacrylate (PMMA). The pressure-bearing capacity of a PMMA-manned cabin was investigated considering the effects of initial geometrical imperfections and large openings. Three types of cabins were studied within the failure mode of nonlinear buckling, including an intact spherical cabin, a spherical cabin with a single opening, and a spherical cabin with double openings. The initial geometrical imperfection ranges from 0.1% to 0.5% of the inner diameter. The ultimate strength decreasing tendency for the different types of cabins with increasing initial imperfection was obtained and the thickness of the hatch cover determined based on the principle of equivalence differed its effects on the strength of the cabin. The influence of the hatch cover stiffness was not linear and indicated the necessity of exploring the coordinated design between the PMMA shell and the metal hatch cover for the transparent cabin.

Keywords: submersible; fully transparent spherical cabin; pressure-resistant shell; PMMA; buckling

check for updates

Citation: Wang, F.; Li, Y.; He, Z.; Zhao, B.; Zhang, J.; Wu, Y. The Ultimate Strength of Fully Transparent Pressure-Resistant Spherical Cabins. *Appl. Sci.* **2023**, *13*, 12229. https://doi.org/10.3390/app132212229

Academic Editor: José António Correia

Received: 17 October 2023
Revised: 4 November 2023
Accepted: 6 November 2023
Published: 10 November 2023

Copyright: © 2023 by the authors. Licensee MDPI, Basel, Switzerland. This article is an open access article distributed under the terms and conditions of the Creative Commons Attribution (CC BY) license (https://creativecommons.org/licenses/by/4.0/).

1. Introduction

In recent decades, deep-sea exploration and development have received increasing attention. The manned submersible (HOV) is an advanced equipment for scientific research and exploration of the deep-sea resources [1]. These submersibles usually need to work in high-pressure and highly corrosive environments, so they are generally designed with an anti-corrosive metal shell structure. In order to facilitate the operator's observation of the external environment, the submersibles will use optical cameras and transparent windows to observe the external environment [2]. However, the narrow perspective of the observation window makes it difficult for the diver to observe, and it can easily lead to blind spots and service delays [3]. Therefore, a fully transparent cabin to improve vision and driving experience is a good practice to expand the range of observation as shown in Figure 1, which is a schematic figure of a submersible with a fully transparent cabin [4].

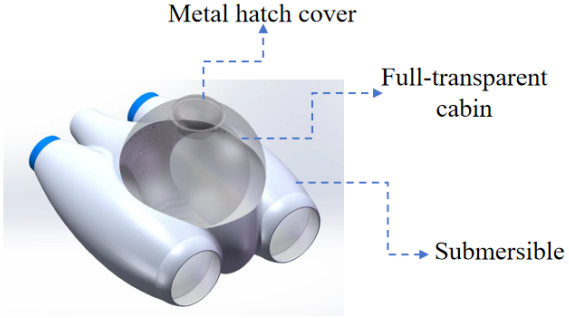


Figure 1. A schematic figure of a manned submersible with fully transparent cabin.

In 1970, the US Navy launched a spherical PMMA submersible called NEMO [5], which means that the concept of using transparent material PMMA to manufacture the entire pressure-resistant shell is completely feasible. After decades of development, fully transparent submersibles have achieved success in the commercial field of sightseeing submersibles, such as the Trion submersible in the United States, C-Quester in the Netherlands, and DW2000 in collaboration with NASA in Canada [6]. Japan has also launched the "Deep Sea 12000" research program, while China put into operation the "Huandao Jiaolong" sightseeing submersible in 2015, making it the world's largest fully transparent passenger-carrying sightseeing submersible [7]. Because of this, the service safety of fully transparent structures is particularly important, whether from a scientific research perspective or with a focus on future commercial value. However, the maturity of the current design is being tested by service experience and the accumulated safety evaluation foundation is insufficient. Stability is a primary concern in the safety evaluation of pressure-resistant structures.

Under the high outside pressure in deep-sea conditions, the pressure-resistant PMMA cabin may fail due to outside pressure exceeding its ultimate strength. The failure modes mainly include yield or fracture caused by insufficient material strength, which is called strength failure, or instability caused by insufficient structural stiffness, which is called buckling failure [8]. Generally speaking, the failure of thin shell structures usually is not related to the issue of strength failure, but thick shell structures may conform to both theories simultaneously. A pressure-resistant cabin requires relevant calculations based on different thicknesses to determine their failure mode, namely strength failure or buckling instability. Under external pressure, researchers have proposed various critical pressure calculation formulas for thick shell structures. Zoelly originally proposed the formula for determining the buckling critical pressure of perfect spherical shells under external pressure [9]. This theoretical formula assumes that the structure is flawless, but various spherical shells manufactured in engineering practice cannot be flawless [10], which makes the buckling critical pressure obtained through experiments much smaller than the theoretical solution [11]. In 1934, Donnell proposed using nonlinear large deflection theory to analyze the post buckling state of thin-walled cylindrical shells when studying the torsional buckling problem [12], established a nonlinear cylindrical shell equation, obtained the critical buckling pressure, and obtained the post buckling waveform of the shell through experiments. In 1941, Based on Donnell's study, Carmen and Qian [13] studied the buckling problem of spherical shells., considering the initial defects of the spherical shell, and achieved breakthrough results. They obtained a formula for calculating the nonlinear buckling critical pressure of the spherical shell. Many scholars, such as Donnell & Wan [14], Koiter [15], Manuel [16], and others, have formed the primary elements of contemporary stability theory via investigation, such as prestress computation and nonlinear big deflection theory. In 2010, during the building of the "Jiaolong" submersible, Pan and Cui [17] presented the empirical formula for the critical pressure of titanium alloy manned submersible pressure shells and brought it into classification society standards [18,19].

The failure modes of stiffened cylindrical shells, such as shell yielding, local buckling of the shell between annular stiffeners, overall buckling of the shell and stiffeners, and interacting buckling modes of local and global bonding, were examined by [20,21]. Other researchers have derived the buckling calculation formula for open shell pressure by analyzing factors such as incision position, aspect ratio, and aspect thickness ratio [22]. It is important to note that the majority of the study mentioned above focuses on the metal structures' pressure-resistant shells. with limited evaluation of the durability of PMMA cabin. At present, small sample testing and numerical analysis are the key areas of study for PMMA cabins [11]. At the same time, there are limited investigation reports on the buckling failure behavior of PMMA spherical pressure cabins [23].

The rapid development of finite element methods provides techniques for analyzing the buckling failure behavior of PMMA spherical cabins. In the present study, the failure

mode and critical pressure of PMMA spherical pressure-resistant cabins based on nonlinear buckling theory were analyzed using finite element analysis. Relevant simulations were conducted to explore the effects of initial geometric defects as well as thickness to radius ratio (t/R) on critical pressure and the effect of the stiffness of the metal hatch cover was investigated. These research results will provide necessary technical references for design of PMMA spherical pressure-resistant cabins.

2. Material Properties

2.1. Specimens and Test Procedure

The PMMA cylindrical specimens were processed in accordance with ASTM D695-15 [24] and ASTM D2990 [25] with Φ 12.7 mm $\times$ l 25.4 mm and a manufacture accuracy of 0.02 mm, as shown in Figure 2. The processed specimen meets the size requirements in specifications. The appearance of the material after compression failure is shown in Figure 3.

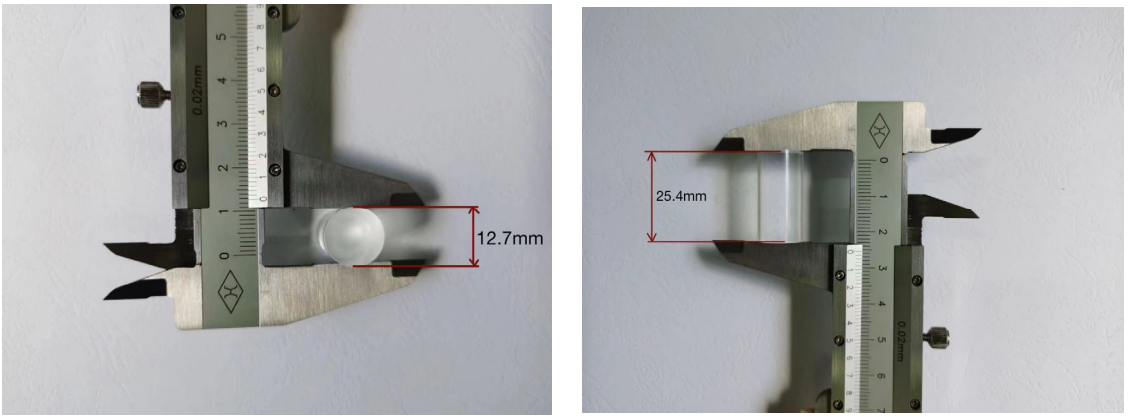


Figure 2. Photos of specimens.



Figure 3. Appearance of material samples after destruction.

2.2. Material Test Results

The main mechanical properties of PMMA are listed in Table 1. Use a microcomputer-controlled electronic universal testing machine TSE105D (WANCE, Shanghai, China) to perform compressive testing of materials, engineering stress and strain can be obtained and converted to the true stress–strain curve for numerical calculation. Based on the experimental data and conversion formula [26], the engineering stress–strain curve and the true stress–strain curve can be drawn in Figure 4.

Table 1. Material Properties of PMMA.

Material Property	Value
Elastic Modulus/MPa	2575
Yield Strength/MPa	126
Poisson's ratio	0.35

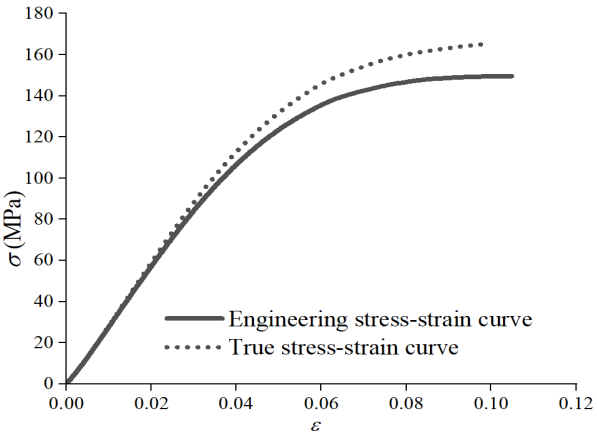


Figure 4. Engineering and true stress–strain curves of PMMA.

3. Ultimate Strength of PMMA Spherical Cabin

3.1. Intact Spherical Cabin

3.1.1. Failure Theory for Intact Spherical Cabin

When the deep-sea submersible is considered, the medium-thick shell is typically used with strength theory. But when the working depth of the submersible is relatively shallow, the thickness of the shell is usually designed as a thin shell, then nonlinear buckling theory of pressure-resistant shell can be applied for calculation. The ratio of thickness to inner radius (t/R) has a boundary point relative to the two sets of theories. The present study is conducted within the scope of nonlinear buckling theory, so for the PMMA cabin, the boundary point should be determined first.

It is easier for the pressure-resistant spherical shell to establish the equilibrium equation in the spherical coordinate system. The maximum stress σ_{max} is generated on the inner surface of the pressure-resistant spherical shell [27].

$$\sigma_{max} = \sigma_i = \frac{3P\left(2+\frac{t}{R}\right)^3}{2\left[\left(2+\frac{t}{R}\right)^3-\left(2-\frac{t}{R}\right)^3\right]} \tag{1}$$

Here, R is the inner radius of the spherical shell and t is of the middle surface of the spherical shell and t is the thickness of the shell; P is the outer uniform pressure acting on the pressure-resistant spherical shell. The pressure gradually increases with the increase of depth, the spherical shell first enters the elastic state, eventually achieves its plastic limit condition after going through the elastic-plastic deformation [28].

The classical definition of buckling can be attributed to the transfer of equilibrium of a structure. When a stable equilibrium state is out of equilibrium after an arbitrarily small, applied disturbance, the structure is thus in an unbalanced state, and this transfer from a stable equilibrium state to an unbalanced state is referred to as the structure buckling. The term "buckling critical pressure" refers to the pressure on the structure in the critical condition and may be written as follows:

$$P = \frac{2Et}{R(1-v^2)}\left\{\frac{(1-v^2)+t^2\left[\xi(2+\xi)+\left(1+v^2\right)/12R^2\right]}{\xi+1+3v}\right\} \tag{2}$$

In the above formula, P is the pressure, E is the elastic modulus, and v is the Poisson's ratio. In the above equation, according to the stable equilibrium condition $dP/d\xi = 0$, substitution into the above equation yields the following:

$$P_{cr} = \frac{2Et}{R(1-v^2)}\left(\sqrt{\frac{(1-v^2)}{3}}\frac{t}{R} - \frac{vt^2}{2R^2}\right) \quad (3)$$

According to above equations, the yield critical pressure and buckling critical pressure of PMMA spherical shell were plotted as a function of t/R ratio, as shown in Figure 5. According to the theoretical formula curve, when $t/R = 0.0424$, the yield critical pressure and buckling critical pressure of the PMMA spherical shell approach to the same point, both of which are 6.06 MPa. In addition, this marks a shift in the PMMA spherical shell's mechanism of failure. The buckling critical pressure is smaller than the yield critical pressure when the t/R ratio is less than 0.0424, causing buckling failure to occur first. Should this not occur, yield failure replaces buckling failure as the mechanism of failure. Therefore, in order to ensure that the intact PMMA spherical shell undergoes buckling failure first, in the subsequent numerical analysis, a tentative design of the PMMA spherical shell with the internal radius $R = 735$ mm and the thickness $t = 29.4$ mm ($t/R = 0.04$) are adopted for analysis.

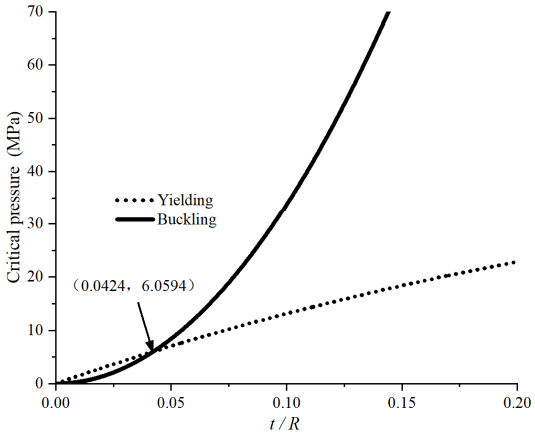


Figure 5. Strength theory and buckling theory formula curve of PMMA spherical shell.

3.1.2. Effect of Initial Geometrical Imperfection

A series of finite element models was used to simulate the eigenvalue buckling and nonlinear buckling of PMMA spherical cabins. Eigenvalue buckling analysis was performed first to obtain the initial geometry imperfection mode as a geometrical shape input required for post-buckling analysis. If the inner radius of the spherical pressure hull was $R = 735$ mm and the thickness was $t = 29.4$ mm, which was applied in the present analysis, then $t/R = 0.04$, which was within the consideration of thin shells [29].

In theory, the pressure shell was not subject to any constraints, but according to the regulations of the classification society [30], three-point constraints are used to restrict the model's displacement in six directions in order to get rid of its stiff displacement. The three-point constraints were used to restrict the stiff displacement of the model, and a pressure of 10 MPa was applied to the spherical shell, as shown in Figure 6. In the material properties section, the material curve was input based on Figure 4, and the element type C3D8R, with a mesh size of 22 mm and hexahedral meshing is adopted for analysis, as shown in Figure 6. Usually, the first-order buckling mode is used as the initial geometrical imperfection of the structure [31].

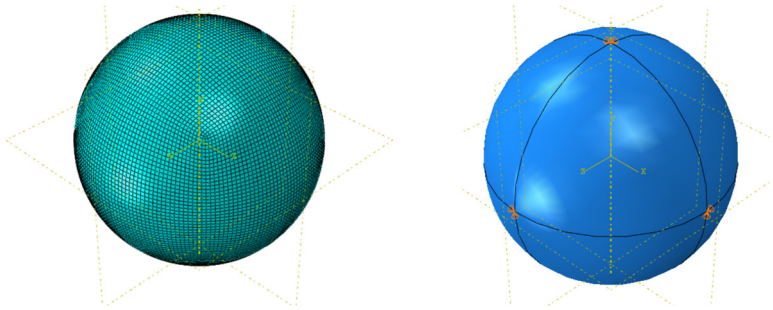


Figure 6. FE model of an intact spherical cabin and boundary conditions.

Although the first-order mode may not necessarily be the worst-case defect situation, it is still a very simple and effective method to determine the defect sensitivity of the structure. Some researchers have also used random methods [32] or *N*-order characteristic defect mode methods [33] to identify the worst-case defect instability mode and calculate the minimum unstable load for structural instability. Nevertheless, rather than concentrating on the worst-case scenario, the current study examines how faults affect the complete spherical shell structure. Therefore, the first order mode is still selected as the initial defect. Figure 7 depicts the post-buckling equilibrium path of PMMA spherical cabin with the imperfection amplitude of 0.5%*R*. The load percentage coefficient, which is produced by standardizing the original applied pressure, is displayed on the vertical axis. The end of the curve corresponds to the post-buckling mode of the spherical shell, and the extreme point represents the critical buckling mode of the spherical shell, which is multiplied by the external pressure to give the critical buckling pressure. The findings indicate that the critical pressure for nonlinear buckling when adding the initial geometrical imperfection of 0.5%*R* is 5.02 MPa, and the linear buckling critical pressure calculated by eigenvalue buckling is reduced by 2.5% from 5.15 MPa, which is 5.8% lower than the theoretical solution of 5.33 MPa. This suggests that the critical pressure value of PMMA spherical cabins is significantly impacted by initial defects.

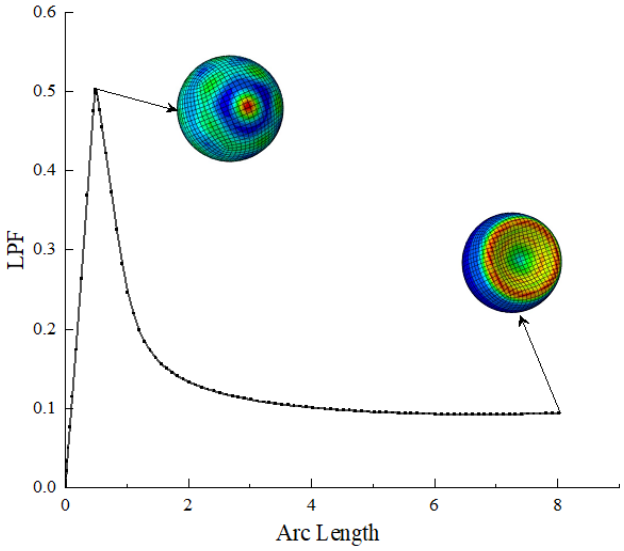


Figure 7. Load Proportional Factor versus Arc Length curve of an intact PMMA spherical cabin.

As the initial geometrical imperfection increases, the critical pressure of the PMMA spherical cabin gradually decreases. Table 2 displays the precise values. When the ultimate strength of the PMMA spherical cabin with different size of initial geometrical imperfection is normalized by its corresponding value with imperfection of 0.1%*R*, Figure 8 can be drawn based on the proportion of strength value reduction, which represents the ultimate strength

reduction trend of the intact PMMA spherical cabin with the increase of geometrical imperfection.

Table 2. Effect of initial geometrical imperfection on ultimate strength of the intact spherical cabin.

t*/*R	**0.04**				
Initial geometrical imperfection	0.1%	0.2%	0.3%	0.4%	0.5%
Theoretical value of the buckling pressure (MPa)	5.33	5.33	5.33	5.33	5.33
Numerical results of buckling pressure (MPa)	5.31	5.21	5.13	5.08	5.02
Failure mode					

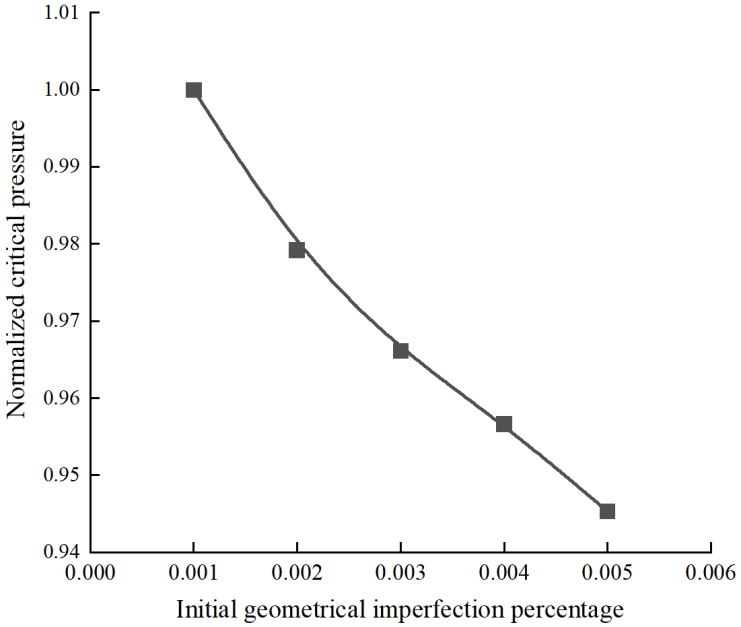


Figure 8. Strength reduction curve with initial geometrical imperfection.

3.2. Spherical Cabin with a Single Access Opening

3.2.1. Numerical Analysis of the Spherical Cabin with a Single Access Opening

When designing submersibles, multiple openings are usually reserved as for personnel entry and exit, electronic equipment installation, etc., and the existence of openings can affect the strength of pressure-resistant structures. The present study conducts corresponding nonlinear buckling numerical analysis considering the design of single and double openings, in order to explore the effect of openings on the ultimate strength of the PMMA cabin. The hatch cover for the opening in the present study is made of aluminum alloy 6061-T6. The thickness is determined based on the principle of equivalence in which it is assumed that the entire spherical shell is made of aluminum 6061-T6 and can withstand pressure greater than the critical pressure of the intact PMMA spherical shell. Based on Section 3.1, As can be observed, the PMMA shell's critical pressure is 5.02 MPa. According to the formula specified in CCS rule, the stress of the entire shell can be calculated as follows:

$$\sigma = \frac{P_j R}{2t} \tag{4}$$

$$\sigma \leq 0.85 R_{eH} \tag{5}$$

where P_j is the calculation pressure (MPa), σ is the Shell plate stress of spherical shell and R_{eH} is the yield stress of the material (MPa). Based on this principle, it can be calculated

that if a complete aluminum alloy shell needs to bear a pressure of 6 MPa, the value of thickness t should be 9.6 mm. Usually, a safety factor of 1.5 is applied for design, which leads to the thickness of 14.4 mm. The specific dimensions are shown in Figure 9.

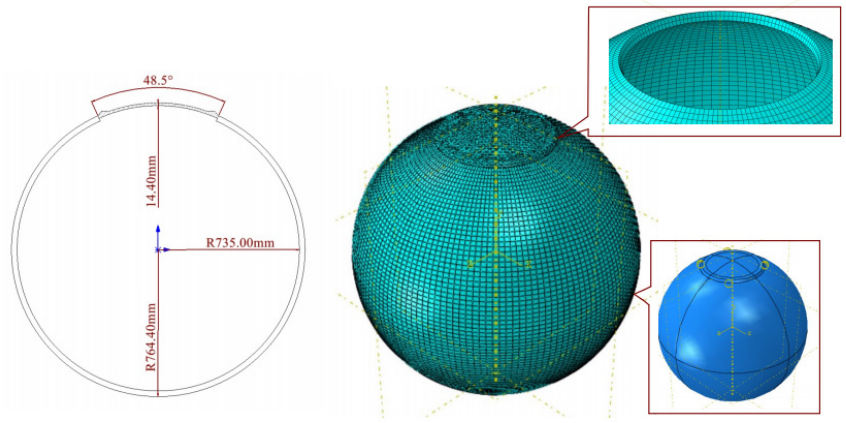


Figure 9. Geometry model and FE model of the PMMA spherical cabin with single access openings.

The procedure of finite element modeling and analysis steps has been described in Section 3.1.1. The element type will be C3D8R, and the shell part will be divided into hexahedral structural meshes. The tetrahedral free-meshing is applied for hatch cover. Then, the critical pressure of the spherical cabin with a single access opening and initial geometrical imperfection of 0.5%R is added to the model, which results in the critical pressure of 3.11 MPa, and reduces the strength of the intact spherical cabin by 38.05%. Its crushing morphology is also significantly different from that of the intact spherical cabin. Figure 10 shows the LPF curve of the PMMA spherical cabin with a single access opening. The stress concentration occurs around the opening, and the final failure also occurs near the connection between the metal hatch cover and the PMMA shell.

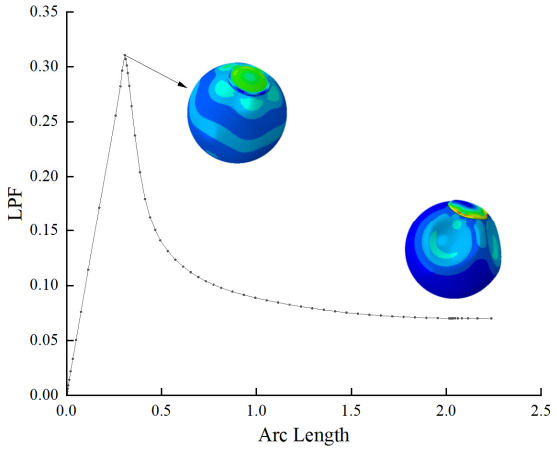


Figure 10. Load Proportional Factor versus Arc Length curve of a PMMA spherical cabin with a single access opening.

3.2.2. Effect of Initial Geometrical Imperfection

Apply initial geometrical imperfection from 0.1%R to 0.5%R to the PMMA spherical cabin with a single access opening for calculation. The results are presented in Table 3. As the initial imperfection gradually increases, its ultimate strength shows a significant downward trend. Taking the ultimate strength with the imperfection of 0.1%R as the benchmark, it can be seen that when the imperfection increases to 0.5%, the ultimate strength decreases by 2.8%, which is relatively small compared to an intact PMMA spherical cabin.

Table 3. Effect of initial geometrical imperfection on ultimate strength of the PMMA spherical cabin with a single access opening.

t*/*R	**0.04**				
Initial geometrical imperfection	0.1%	0.2%	0.3%	0.4%	0.5%
Numerical results of buckling pressure (MPa)	3.2	3.18	3.15	3.13	3.11
Failure Mode					

Attempting to gradually thicken the PMMA spherical shell to approach the ultimate strength of an intact spherical shell, the critical pressure values are calculated based on three thickness to diameter ratios of 0.04, 0.05, and 0.06. It was found that when t/R = 0.05, it is already close to the intact spherical shell. Then, increasing the thickness to diameter ratio at a spacing of 0.001 resulted in the calculation of the critical pressures of 0.051, 0.052, and 0.053 showing that t/R of the spherical cabin with a single access opening had a relatively close ultimate strength to the intact spherical shell when being thickened to 0.051–0.052, as shown in Figure 11.

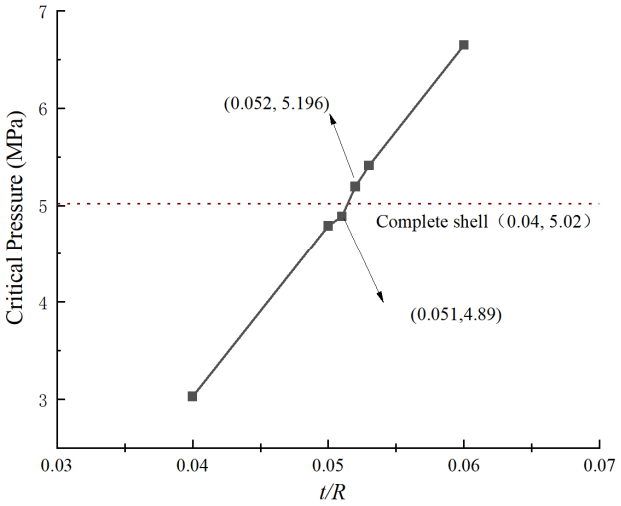


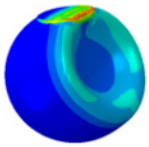
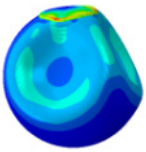
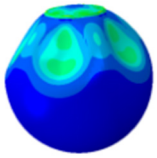
Figure 11. Critical pressure changes the tendency at different t/R of the spherical cabin with a single access opening.

3.2.3. Effect of Hatch Stiffness

In the previous section, it was found that increasing the thickness can improve the ultimate strength of the PMMA spherical cabin with a single access opening. When the spherical cabin constitutes a PMMA shell and a metal hatch cover, to investigate whether increasing the thickness of the hatch cover can improve the ultimate strength of the pressure-resistant shell, a comparison is made by changing the thickness of the metal hatch cover in the range of 9.6 mm, 14.4 mm, and 19.2 mm to vary the stiffness of the hatch cover. The thickness is changed by using different safety factors, of which 14.4 mm is considering the safety factor of 1.5 and 19.2 mm is for the safety factor of 2.0. The finite element calculation results are shown in Table 4.

Based on the calculation results, increasing the thickness of the hatch cover within a certain range can improve the overall strength of the spherical cabin. However, blindly increasing the thickness does not necessarily enhance the structural strength. A metal hatch cover that is excessively thick may actually weaken the structure since the entrance wall's strong restrictions will deteriorate before the PMMA shell fails.

Table 4. Effect of hatch thickness on ultimate strength of the PMMA spherical cabin with a single access opening.

t*/*R	**0.04**		
Cover thickness (mm)	9.6	14.4	19.2
Numerical results of buckling pressure (MPa)	3.05	3.11	2.69
Failure Mode			

3.3. Spherical Cabin with Double Access Openings

A spherical cabin model with double access openings is established for analysis, and the size of which is consistent with "Section 3.2.1" as well as the design criteria for access opening design. The whole structure will be designed symmetrically, but with different opening angles of 48.5° and 44°, respectively, as indicated in Figure 12. The mesh size remains consistent at 22 mm, and the mesh element type is C3D8R.

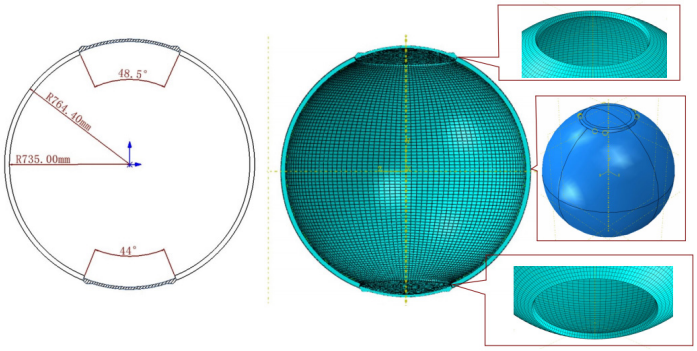


Figure 12. Geometry model and FE model of the spherical cabin with double access openings.

3.3.1. Effect of Initial Geometrical Imperfection

In order to ensure the convergence of the calculation results, double-layer meshes are divided into two hatch cover parts for the PMMA spherical cabin with double access openings. The initial geometrical imperfection was added from 0.1%*R* to 0.5%*R*. The calculation results of nonlinear buckling analysis are listed in Table 5, which shows an overall trend of almost linearly decreasing with initial geometry imperfection. This also indirectly verifies the correctness of the previous conclusion for the ultimate strength decreasing trend. The final failure mode of a spherical cabin with double access openings is different from that of the intact spherical shell and the spherical cabin with a single access opening, as shown in Figure 13. Stress concentration occurs in the vicinity of the two access openings.

Table 5. Effect of initial geometrical imperfection on ultimate strength of the spherical cabin with double access openings.

t*/*R	**0.04**				
Initial geometrical imperfection	0.1%	0.2%	0.3%	0.4%	0.5%
Numerical results of buckling pressure (MPa)	3.32	3.29	3.26	3.23	3.21
Failure Mode					

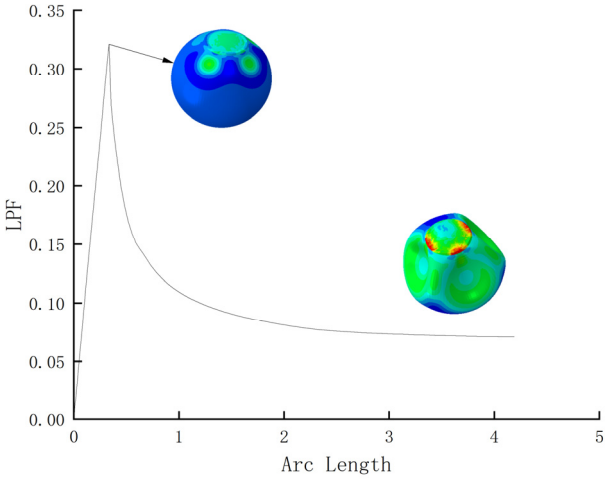


Figure 13. Load Proportional Factor versus Arc Length curve of a PMMA spherical cabin with double access openings.

3.3.2. Effect of Hatch Stiffness

In Section 3.2, it was observed that an increase in the thickness of the hatch cover can improve the structural strength within a certain range, but blindly increasing the thickness can actually reduce the structural strength. To verify whether the PMMA spherical cabin with double access openings conforms to the above conclusion, the analysis for the present case was conduced with hatch cover thicknesses at 9.6 mm, 14.4 mm, and 19.2 mm, and the inner and outer diameters consistent with Section 3.2. The calculation results are shown in Table 6. It can be clearly seen from the data that when the thickness of the hatch cover increases from 9.6 mm to 14.4 mm, the critical pressure increases from 3.06 MPa to 3.21 MPa, with an increase in strength of about 4.9%. Continuing to increase the thickness of the hatch cover to 14.4 mm, the structural strength does not further improve, but decreases to 3.08 MPa, which better verifies the correctness of the previous conclusion. In the future's study, further work should be done to explore the coordinated design between the PMMA shell and the metal hatch cover.

Table 6. Effect of hatch thickness on ultimate strength of the PMMA spherical cabin with double access openings.

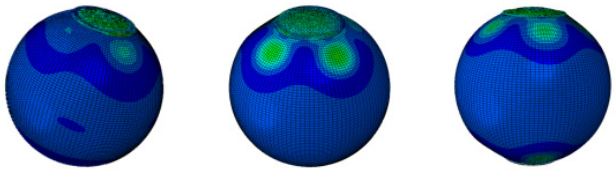
t*/*R	**0.04**		
Cover thickness (mm)	9.6	14.4	19.2
Numerical results of buckling pressure (MPa)	3.06	3.21	3.08
Failure Mode			

Figure 14 shows the comparison of strength reduction tendency for three cases with initial geometrical imperfections. Access openings will change the strength reduction tendency. The sensitivity of initial geometrical imperfections can be reduced. Under the maximum initial geometrical imperfection level of 0.5%R required by the China Ship Classification Society (CCS, 2018), the effects of normalized critical pressure is reduced by at least 2.56%.

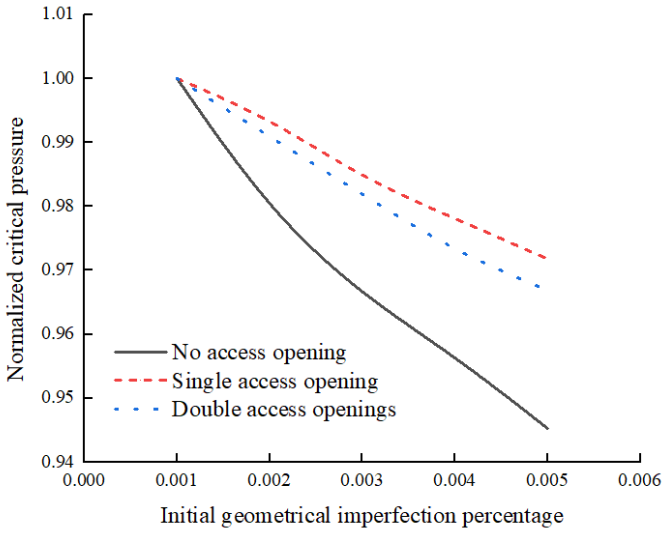


Figure 14. Comparison of strength reduction tendency with initial geometrical imperfections.

4. Summary and Conclusions

The ultimate strength of a fully transparent spherical cabin made of PMMA is studied by taking the initial geometrical imperfection and metal cover stiffness into account. The boundary point of t/R between strength failure and buckling failure of PMMA spherical cabin through classical theoretical formulas is determined first as the present study aims at investigation within the range of buckling mode. When t/R of the PMMA spherical hull is less than 0.0424, buckling failure occurs first ahead of strength failure. Based on that, a series of numerical models including the intact spherical cabin, spherical cabin with a single access opening, spherical cabin with double access openings are established and the eigenvalue buckling results were introduced into the initial imperfection shape for nonlinear buckling analysis. The changing tendency of critical buckling pressure was observed with varieties of the initial geometrical imperfections and t/R.

Results show that the critical pressure has a decreasing trend as the initial geometrical imperfection increases, and that the intact spherical cabin shows the greatest decrease, indicating a higher sensitivity to initial imperfection. The critical buckling pressure linearly increases with the increase of t/R for PMMA spherical cabin with access openings. The reduction extent of the spherical cabin with a single access opening is smaller than that with double access openings, indicating the strength sensitivity of PMMA spherical cabins to initial imperfections and openings. Moreover, for PMMA pressure-resistant cabin, the thickness of the metal hatch cover also significantly affects its critical pressure. Within a certain range, the strength of the spherical cabin will increase with the increase of hatch cover thickness. However, a metal cover that is too thick will reduce its structural strength due to the constraints at the contact between the cover hatch cover and the PMMA shell. It is absolutely necessary to determine a reasonable range of hatch cover thicknesses in the future. Coordinated design is compulsory and subsequent improvements can be made by aiming at improving the simulation accuracy and locally refined structure design to reduce the stress concentration effect which will be fully considered for safety evaluation.

Author Contributions: Methodology, F.W.; Software, Y.L., Z.H. and B.Z.; Validation, J.Z.; Formal analysis, Y.L. and Z.H.; Investigation, F.W. and Y.L.; Data curation, Z.H., B.Z. and J.Z.; Writing—original draft, F.W.; Writing—review & editing, Y.W.; Supervision, F.W.; Project administration, F.W.; Funding acquisition, F.W. All authors have read and agreed to the published version of the manuscript.

Funding: The National Key Research and Development Program of China provides funding for this work. (Grand No. 2021YFC2800600), National Natural Science Foundation of China (Grant No. 52071203), The authors would like to thank Shanghai High-level Local University's Fishery Engineering and Equipment Innovation Team for their support, as well as the Open Fund of the Fujian Province Key Laboratory of Ship and Ocean Engineering.

Data Availability Statement: The data can be provided by the corresponding authors when needed. The data are not publicly available due to privacy.

Conflicts of Interest: The authors declare that they have no known competing financial interest or personal relationships that could have appeared to influence the work reported in this paper. The funders had no role in the design of the study; in the collection, analyses, or interpretation of data; in the writing of the manuscript; or in the decision to publish the results.

References

1. Luo, S.; Li, Y.S.; Wang, W.B. Development and prospects of non-metallic submersible pressure hull. *Chin. J. Ship Res.* **2020**, *15*, 9–18.
2. Guo, D.Y.; Huang, X.P.; Wang, F. The Creep Properties and Numerical Simulation for PMMA Window. *J. Shanghai Jiaotong Univ.* **2019**, *53*, 513–520.
3. Lu, B.; Liu, T.; Cui, W.C. Ultimate strength of pressure spherical hull in deep-sea manned submersibles. *J. Ship Mwchanics* **2004**, *8*, 51–58.
4. Li, W.Y.; Wang, S.; Liu, T.; Shen, Y.S.; Ye, C. Current Status and Progress on Pressure Hull Structure of Manned Deep Submersible. *Ship Build. China* **2016**, *57*, 210–221.
5. Das, P.S. Redesign of NEMO-type spherical acrylic submersible for manned operation to 3000 ft (914 m) ocean depth. *J. Press. Vessel Technol.-Trans. ASME* **2002**, *124*, 97–107. [CrossRef]
6. Wang, F.; Wang, W.W.; Zhang, Y.K.; Du, Q.H.; Zhang, J.; Cui, W.C. Effect of Temperature and Nonlinearity of PMMA Material in the Design of Observation Windows for a Full Ocean Depth Manned Submersible. *Mar. Technol. Soc. J.* **2019**, *53*, 27–36. [CrossRef]
7. Liu, S.; Ye, C.; Tang, G.W.; Cheng, F.; Jiang, L. Design and Development of the First Acrylic-hulled Submersible in China. *Ship Build. China* **2019**, *60*, 113–120.
8. Wu, Y.; Li, Y.J.; Luo, R.L.; Zhang, Z.G.; Wang, F.; Zhao, B.X.; Yang, C.; Zhang, J.F.; Gaidai, O. Failure analysis on fully-transparent deep-sea pressure hulls used at 2,500 m depth. *Front. Mater.* **2023**, *9*, 1099610. [CrossRef]
9. Zoelly, R. *Über ein Knickungsproblem an der Kugelschale*; Zürcher & Furrer: Zürich, Switzerland, 1915.
10. Zhu, Y.M.; Liang, W.W.; Zhao, X.L.; Wang, X.R.; Xia, J. Strength and stability of spherical pressure hulls with different viewport structures. *Int. J. Press. Vessel. Pip.* **2019**, *176*, 13. [CrossRef]
11. Rajput, N.S.; Pranesh, S.B.; Sathianarayanan, D.; Ramadass, G.A. Acrylic spherical pressure hull for Manned Submersible. *Mater. Today: Proc.* **2021**, *46*, 9412–9418.
12. Jiao, P.; Chen, Z.; Ma, H.; Ge, P.; Gu, Y.; Miao, H. Buckling behaviors of thin-walled cylindrical shells under localized axial compression loads, Part 1: Experimental study. *Thin-Walled Struct.* **2021**, *166*, 108118.
13. Kármán, T.V.; Tsien, H.S. The buckling of thin cylindrical shells under axial compression. *J. Aeronaut. Sci.* **2003**, *40*, 898–907.
14. Donnell, L.H.; Wan, C. Effect of imperfections on buckling of thin cylinders and columns under axial compression. *J. Appl. Mech.* **1950**, *17*, 73–83. [CrossRef]
15. Koiter, W.T. On the Stability of Elastic Equilibrium. Ph.D. Thesis, Technical University at Delft, Amsterdam, The Netherlands, 1945.
16. Stein, M. *The Influence of Prebuckling Deformations and Stresses on the Buckling of Perfect Cylinders*; NASA: Washington, DC, USA, 1964.
17. Pan, B.B.; Cui, W.C. An overview of buckling and ultimate strength of spherical pressure hull under external pressure. *Mar. Struct.* **2010**, *23*, 227–240.
18. Pan, B.B.; Cui, W.C.; Shen, Y.S.; Liu, T. Further study on the ultimate strength analysis of spherical pressure hulls. *Mar. Struct.* **2010**, *23*, 444–461. [CrossRef]
19. *GB 150*; Design of Pressure Vessels. Standardization Administration of China: Beijing, China, 2011.
20. Cho, S.R.; Muttaqie, T.; Do, Q.T.; Kim, S.; Kim, S.M.; Han, D.H. Experimental investigations on the failure modes of ring-stiffened cylinders under external hydrostatic pressure. *Int. J. Nav. Archit. Ocean. Eng.* **2018**, *10*, 711–729.
21. Cho, S.R.; Muttaqie, T.; Do, Q.T.; Park, S.H.; Kim, S.M.; So, H.; Sohn, J.M. Experimental study on ultimate strength of steel-welded ring-stiffened conical shell under external hydrostatic pressure. *Mar. Struct.* **2019**, *67*, 26.
22. Shariati, M.; Rokhi, M.M. Numerical and experimental investigations on buckling of steel cylindrical shells with elliptical cutout subject to axial compression. *Thin-Walled Struct.* **2008**, *46*, 1251–1261.
23. Zhu, Y.; Dong, J.H.; Gao, B.J. Buckling Analysis of Thin Walled Cylinder with Combination of Large and Small Stiffening Rings under External Pressure. *Procedia Eng.* **2015**, *130*, 364–373. [CrossRef]
24. *ASTM D695-15*; Standard Test Method for Compressive Properties of Rigid Plastics. ASTM International: West Conshohocken, PA, USA, 2015.
25. *ASTM D2990*; Standard Test Methods for Tensile, Compressive, and Flexural Creep and Creep-Rupture of Plastics. ASTM International: West Conshohocken, PA, USA, 2011.
26. Zhang, M.; Zhang, J.; Tang, W.X.; Wang, W.B.; Gao, J. Experimental and theoretical investigation on buckling of spherical shells. *J. Jiangsu Univ. Sci. Technol.* **2018**, *32*, 627–632.
27. Liu, D.; Zhu, H.T.; Liu, F.; Cao, J.Q.; Ding, Z.J.; Zhang, Y. Buckling failure analysis of PMMA spherical pressure hull. *Ocean Eng.* **2022**, *245*, 8. [CrossRef]

28. Xu, B.Y.; Liu, X.S. *Applied Elasticity*; Tsinghua University Press: Beijing, China, 1995. (In Chinese)
29. Zhu, Y.M.; Ma, Q.L.; Dai, Y.; Zhang, J. Mechanical properties and fatigue analysis of spherical pressure shell with openings. *Ship Sci. Technol.* **2017**, *39*, 7–11.
30. CCS. *Rules for Classification of Diving Systems and Submersibles*; China Communications Press: Beijing, China, 2018.
31. Sosa, E.M.; Godoy, L.A.; Croll, J.G.A. Computation of lower-bound elastic buckling loads using general-purpose finite element codes. *Comput. Struct.* **2006**, *84*, 1934–1945. [CrossRef]
32. Taheri-Behrooz, F.; Omidi, M.; Shokrieh, M.M. Experimental and numerical investigation of buckling behavior of composite cylinders with cutout. *Thin-Walled Struct.* **2017**, *116*, 136–144. [CrossRef]
33. Shen, J.; Yang, J.; Ma, H.B. Static stability anaysis of K8 single-layer ellipsoid reticulated shell. *Spat. Struct.* **2009**, *15*, 69–72.

Disclaimer/Publisher's Note: The statements, opinions and data contained in all publications are solely those of the individual author(s) and contributor(s) and not of MDPI and/or the editor(s). MDPI and/or the editor(s) disclaim responsibility for any injury to people or property resulting from any ideas, methods, instructions or products referred to in the content.